INTERFACIAL BEHAVIOR OF RNA-FREE MS2 BACTERIOPHAGE PARTICLES

BY

NICKOLAS JOSEPH EASTER

THESIS

Submitted in partial fulfillment of the requirements
for the degree of Master of Science in Environmental Engineering in Civil Engineering
in the Graduate College of the
University of Illinois at Urbana-Champaign, 2011

Urbana, Illinois

Adviser:

Professor Thanh Helen Nguyen

Abstract

The effect of genomic material on the effective surface charge a viral capsid was investigated in this study. The RNA of bacteriophage MS2 was removed and the empty capsid characterized and compared to intact MS2. Transmission electron microscopy was used to ensure that the MS2 capsid was intact and RNA removed. Electrophoretic mobility, aggregation kinetics and kinetics of deposition on silica surface were studied for these two nanoparticles. The isoelectric point of MS2 and RNA-free MS2 were found to be 3.4 and 3.2 respectively, found by varying pH at a constant ionic strength. The electrophoretic softness, found by varying ionic strength and constant pH, found that MS2 was 2.1 nm and that RNA-free MS2 was 1.6 nm, a slightly harder particle. Electrophoretic mobility results of these two particles are similar in solution containing Na^{+} or Ca^{2+} or Mg^{2+} up to ionic strength of 600 mM. Similar aggregation kinetics of MS2 and RNA-free MS2 measured by time-resolved dynamic light scattering at increasing ionic strengths of Na^{+}, Ca^{2+} and Mg^{2+} cations were observed. No significant aggregation was observed for both types of particles in solutions containing up to 600 mM NaCl. Insignificant aggregation at high ionic strength suggests an important role of steric repulsion. Using a Quartz Crystal Microbalance, RNA-free MS2 attachment efficiency was found to be higher than MS2. This can be explained by more steric repulsion by the untreated MS2 particles. Similarity in electrophoretic mobility and aggregation of these two particles suggest that for non-magnetic nanoparticles, surface properties are dominant.

Acknowledgements

This research was completed with the support of WaterCAMPWS, the Center of Advanced Materials for the Purification of Water with Systems and the National Science Foundation career agreement #0954501. This work was done in collaboration with Professor Steven Mylon of the Chemistry Department at Lafayette College. Thanks to my adviser, Professor Thanh Helen Nguyen for her guidance in experimentation and interpretation and for providing me the opportunity to further educate myself. Thanks to Leonardo Gutierrez for all of his assistance, tutoring, and taking the time to teach me the techniques necessary to complete this project. Leonardo should also be recognized for his work in replicating some the EPM experiments, performing aggregation for MS2 and RNA-free MS2 in Na^+, aggregation of MS2 in Ca^{2+}, and deposition of MS2 and RNA-free MS2 onto silica in Na^+. Finally, thanks to the remainder of the Environmental Bio-Interface (EBI) group for their support and allowing me to learn of their experiences.

TABLE OF CONTENTS

CHAPTER 1

INTRODUCTION

As the field of nanotechnology grows and combines more technical disciplines, so does the need to better understand the properties and consequences of that technology interacting with biological systems (Nel et al. 2009). This requires an understanding of the fundamental relationships that govern the colloidal and interfacial behavior of nanoparticles. Currently, the initial model used to help predict the colloidal and interfacial behavior of rigid nanoparticles (e.g. metal oxides) is Derjaguin-Landau-Verwey-Overbeek (DLVO) theory (Elimelech et al. 1995). While DLVO theory maybe able to accurately model rigid nanoparticle behavior (Chen et al. 2006), it cannot accurately predict the complex interactions of "soft" particles (e.g. viruses, bacteria, natural organic matter) (Mylon et al. 2009, Langlet et al. 2008, Ohshima 1995). Even recent advances to DLVO theory to account for some of these complex interactions fail to adequately model the behavior of "soft" particles, which can be partly attributed to the heterogeneous polymer layers that make up the surface portion of the "soft" particle. These layers invoke a synergistic combination of steric and electrosteric interactions, as well as offer multiple points for which complexation can occur with charged particles in the environment. DLVO theory is only an approximate model made to take into account electrostatic and van der Waals forces as simple, separate interactions and is not made to take into account these complex systems.

Viruses are naturally occurring bionanoparticles that are pathogenic for a wide array of organisms and are responsible for the vast majority of waterborne diseases (Yoder at al. 2008, Abbaszadegan et al. 2003). While morphology may differ between each virus, each virus usually has a protein shell, or capsid, encapsulating a genome. This consistent structure provides

a well defined, multilayered nanoparticle, and allows for freedom to design their surface properties through genetic engineering or chemical conjugation (Fischlechner et al. 2007). This can allow for empty viral capsids or virus like particles (VLPs), which have a range of uses in material science, engineering, and medicine (Udit et al. 2009, Laufer et al. 2009, Brown et al. 2009, Garcea et al. 2004, Lee et al. 2009). This growing use of bionanoparticles requires a better understanding of the colloidal and interfacial behavior of soft matter, however much of the early research focuses on the bulk effects (Thompson et al. 1999, Loveland et al. 1995, Lipson et al. 1984, Lance et al. 1984, Labelle et al. 1979, Floyd et al. 1977, 1978, 1979, Dowd et al. 1998) with little focus on the nature of the interactions on the nano or molecular scale. DLVO theory is still used as the first approximation of the interfacial interactions in deposition between viruses and mineral surfaces, which incorrectly assumes that the virus is a hard particle and provides an inaccurate model (Pham et al. 2009, Yuan et al. 2009). DLVO cannot be applied to viruses as the electrohydrodynamic interactions are complicated by the unrelated anisotropies of the hydrodynamic permeability and charge density, and due to the complex electrostatic interactions, cannot allow for an accurate prediction of the double layer interactions (Langlet et al. 2008). As such, no accurate model for the soft particle interactions at interfaces exists and the attempts made to model require support from experimental data.

Recent studies have looked at the electrostatic interactions of viral adsorption to solid interfaces, virus-virus aggregation, and the electrokinetics of viruses in a charged field. Studying the deposition of bacteriophage MS2 onto bare silica and natural organic matter, Yuan et al. (2008) showed that increasing ionic strength resulted in increased deposition rates due to charge screening, and Pham et al. (2009) showed similar behavior, but that different divalent cations form different types of complexations with the MS2, with Ca^{2+} being more favorable than Mg^{2+}.

Recent research on Rotavirus where both deposition of virus onto a bare silica surface and natural organic matter as well as the virus/virus aggregation were measured, Gutierrez et al. (2010) found similar results to that of MS2, with increasing ionic strength resulting in increasing deposition, and with an increasing ionic strength creating more significant aggregation until a critical coagulation (CCC) point is reached. Also, the author found that, similar to the MS2 research, that the divalent cation Ca^{2+} caused more favorable deposition and aggregation than Mg^{2+}. The effects of divalent cations on the aggregation and deposition behavior of MS2 and Rotavirus are probably due to the complexation to charged moieties on the virus surface that might alter its conformation. Herath et al. (1999) found that as the pH of a solution approached the isoelectric point (IEP) of a specific virus, the microfiltration membranes rejected a greater percentage of the virus particles in solution. This was attributed to a higher degree of virus/virus aggregation resulting from the decreased electrostatic interactions at the IEP. Langlet et al. (2008) measured the decreases in the mean apparent diffusion coefficient of virus suspensions with decreasing pH using dynamic light scattering (DLS) and confirmed that virus/virus aggregation resulted from decreases in electrostatic repulsive intereactions as the IEP of the virus was approached. Mylon et al. (2009) found that the bacteriophage MS2 exhibited extreme stability against aggregation in the presence of high concentrations of monovalent cations, which would suggest strong steric and electrosteric stabilization of MS2.

Through strictly controlled experiments that examines the colloidal and interfacial behavior of a model set of virus and VLPs, we can improve our understanding of the interactions that occur at soft particle interfaces. Bacteriophage MS2 is a simple single-stranded RNA (ssRNA) virus and a great waterborne nanoparticle in which to study the colloidal and interfacial behavior. The wild-type MS2 capsid is comprised of 180 copies of a single coat protein, which

is assembled in an icosahedral arrangement that is 27 nm in diameter. More importantly, the capsid has 32 pores that are 1.8 nm in diameter that allow for access to the interior of the capsid, allowing for some exposure of the interior ssRNA, and this exposure allows the RNA to be easily removed by alkaline hydrolysis to create an empty capsid (Hooker et al. 2003). With wild-type MS2 and the empty capsid of MS2, or RNA-free MS2, we could directly compare the colloidal and interfacial behavior of the viral capsid with its RNA core intact directly to its empty capsid counterpart and get a better fundamental understanding in what role the core plays in the interfacial interactions.

The objective of this research is to investigate the effects of the single stranded RNA on the surface characteristics of the MS2 bacteriophage. Experiments will include electrophoretic mobility to study particle charge, and time resolved dynamic light scattering to study particle-particle aggregation, both using a zetasizer and controlling the ionic strength with NaCl, $MgCl_2$, and $CaCl_2$. Looking at the particles with a transmission electron microscope to measure particle diameter and ensure the hollow capsid is intact. The virus-solid interface will be studied by measuring deposition kinetics of particles onto a silica surface in the presence of monovalent (Na^+) and divalent (Ca^{2+}) cations using a quartz crystal microbalance coupled with a radial stagnation point flow system. The information measured from the various experiments will be compared to calculated DLVO energy barriers to observe the model's effectiveness in predicting the particle interaction. This knowledge will help form a more fundamental understanding of the viral capsid and the influence the genome has on the colloidal and interfacial behavior of the virus.

CHAPTER 2

MATERIALS AND METHODS

2.1 Solution Chemistries and Reagents

Millipore water (Millipore, Barnstead, USA) of an 18 MΩ-cm resistivity at an unadjusted pH of 5.9 was used for preparing all the solutions for MS2 and RNA-free MS2 deposition and aggregation experiments and electrophoretic mobility measurements. NaOH, HCl, NaCl, $CaCl_2$, $MgCl_2$, poly-L-lysine (PLL) hydrobromide and HEPES of analytical grade were utilized.HEPES buffer was prepared using 100 mM NaCl and 10 mM N-(2-hydroxyethyl) piperazine-N′-2-ethanesulfonic acid at a final pH of 5.9. PLL hydrobromide solution was prepared with HEPES buffer at a final concentration of 0.1 g/L. Before use, electrolyte solutions and HEPES buffer were filtered through a 0.22 μm sterile cellulose acetate membrane. The pH of solutions were adjusted with 0.1 M NaOH and 0.1 M HCl.

2.2 MS2 and Hollow MS2 Preparation and Plaque Forming Units (PFU)

Bacteriophage MS2 (ATCC) were grown in *Escherichia coli* (ATCC) as the host following the propagation procedure described elsewhere (Gutierrez et al. 2009). Briefly, *Escherichia coli*(*E. Coli*) were grown in 300 ml tryptic soy broth solution under incubation conditions (37^oC) until reaching an optical density of 1.0 at 600 nm wavelength, and subsequently inoculated with MS2. Concentration and purification process of MS2 was conducted following the next modified procedures (Gutierrez et al. 2009, Kitis et al. 2003). After lysis, broken cells of *E. coli* were separated from MS2 by sequential steps of centrifugation (5000 RPM) and filtrationthrough a 0.22mm and 0.05 mm low protein binding polycarbonate membrane (Whatman Nucleopore, USA). The MS2 suspension was concentrated using a 100 KDa membrane (Koch Membranes, USA) in a Millipore ultra-filtration unit (Whatman

Nucleopore, USA) to a final volume of 30 ml. Poly(ethylene glycol)-6000 and NaCl were added to the MS2 suspension to a final concentration of 10% (w/v) and 0.5 M respectively and subsequently precipitated by centrifugation at 10,000 rcf for 1 hour. While the supernatant was discarded, the pellet was resuspended in a previously 0.22 μm filtered 1 mM NaCl solution at an unadjusted pH of 5.9. The purified MS2 stock was stored at 4°C at a concentration of ~10^{12} PFU ml^{-1}.MS2 enumeration was conducted following plaque forming unit (PFU) infectivity assaydescribed previously (Gutierrez et al. 2009, Adams 1959). Aseptic conditions were maintained by using a laminar flow hood at every step of the propagation and purification process.

The procedure for RNA removal from MS2 were conducted by adding the next steps (Hooker et al. 2003). After MS2 precipitation by centrifugation at 10,000 rcf for 1 hour,the supernatant was discarded but the pellet was resuspended in a 100 mM Na_2HPO_4 and 100 mM NaCl solution at pH 11.8 and exposed to this alkaline condition for a period of 4 hours at room temperature. The degraded genome by means of phosphate hydrolysis were separated from the RNA-free MS2 suspension using a 100-kDa membrane (Koch Membranes, USA) in a Millipore ultrafiltration unit (Whatman Nucleopore, USA) continuously fed with a previously 0.22 μm filtered 1 mM NaCl solution at an unadjusted pH of 5.9.

2.3 Transmission Electron Microscopy (TEM)

Electron micrographs of MS2 and RNA-free MS2 samples were investigated using TEM by conventional negative staining with uranyl acetate. MS2 or RNA-free MS2 samples were directlyadsorbed onto 300 mesh holey-carbon-coated copper grid. Grids were suspended on a drop of viral solution for 15 minutes and afterwards the dexcess of liquid withdrawn with filter paper. The grid was let dry for 20 minutes at ambient temperature and subsequently the stain

was applied. Micrographs were recorded on a cryo TEM (JEM-2100, JEOL, Tokyo, Japan) operating at 200 kV at high magnification.

2.4 UV Spec Measurements

Concentration of the MS2 and RNA-free MS2 in solution were analyzed through the use of optical density using a Shimadzu UV-2450 ultraviolet-visible spectrophotometer operated in dual beam mode. The spectrophotometer quartz cells were of a useable range of 170 to 2700 nm and 10 mm path length (1Q10, Starna, USA) were used. MS2 and RNA-free MS2 stocks were sampled in dilutions of 10 to 100-fold in 1 mM NaCl solution. The absorbance of viral suspension were measured at a wavelength of 260 nm referenced against 1 mM NaCl solution. The average UV absorbance of each measurement was calculated with no less than 3 sample measurements.

Since RNA-free MS2 was rendered non-infectious after the RNA extraction process, its concentration cannot be measured by infectivity assays. Absorbance was utilized for protein concentration comparison between MS2 and RNA-free MS2. The calculation of the MS2 and RNA-free MS2 particle concentrations in solution took in consideration previous studies such as the optical density of 1.0 at wavelength 265 nm of purified MS2 is a protein density of 130 μg of protein/mL (Legendre et al. 2005), and the molecular weight of MS2 is 3.6×10^6 g/mol (Kuzmanovic et al. 2003), determined by classical light scattering. In addition to the previous studies results, the infectivity assays were conducted for the 10 and 100-fold diluted MS2 samples and the results were correlated to the MS2 absorbance.

2.5 Electrophoretic Mobility (EPM) Measurements

EPM of MS2 and RNA-free MS2 in solution was measured over a wide range of monovalent and divalent salt concentrations (0.1 mM to 600 mM for Na^+, and 0.1 mM to 200

mM for Ca^{2+} and Mg^{2+}) at unadjusted pH of 5.9 using a ZS90 Zetasizer instrument (Malvern, UK). For statistical purposes, at least 3 measurements were conducted for every electrolyte concentration conditionusing clear disposable cells (DTS1060C, Makvern, UK) of 1 ml capacity. MS2 and RNA-free MS2 were added to these solutions to a final optical density of 2.145 and 2.150 respectively at 260 nm wavelength, which ensured an optimal signal for electrophoresis measurements.Isoelectric points (IEP) of MS2 and RNA-free MS2 in 1 mL NaCl were determined by measuring EPM over a wide range of pH from 2.7 to 9.6. For every pH condition,a minimum of 3 measurements were conducted.pH was adjusted using high grade hydrochloric acid (0.1 M HCl) and sodium hydroxide (0.1 M NaOH).

2.6 Time-Resolved Dynamic Light Scattering (DLS) Aggregation Kinetics Experiments

Hydrodynamic diameter of MS2 and RNA-free MS2 were measured before every aggregation experiment for establishing initial baselines (D_{ho}) using a ZS90 Zetasizer instrument (Malvern, UK).This equipment used a 4 mWHeNe laser operating at a wavelength of 633 nm while the scattered light intensity was measured by a photodiode located at 90^{o} from the incident laser beam.MS2 and RNA-free MS2 were added to low volume disposable sizing cuvettes of 500 μL capacity (ZEN0112, Malvern) to a final optical density of 0.215 and 0.215 respectively for Ca^{2+} and Na^{+}, 0.215 and 0.219 respectively for Mg^{2+} all at 260 nm wavelength. At least 3 measurements per sample were conducted before the addition of salt in solution.

2.7 Quartz Crystal Microbalance with Dissipation (QCM-D) Deposition Experiments

We used a QCM-D300 system (Q-Sense AB, Gothenburg, Sweden) to measure deposition kinetics of hydrated MS2 and RNA-free MS2 particles onto a hydrated bare silica surface. The QCM-D allows real time monitoring of the changes in vibrational frequency as wet mass deposits on the quartz crystal sensor. As wet mass deposits onto the sensor, the frequency

of vibration decreases. The wet mass deposition onto the sensor is proportional to changes in resonance and overtone frequencies, the rate of mass deposition in represented by the rate of frequency shift. We monitored the shifts in normalized third overtone frequency ($\Delta f_{(3)}/3$) to determine the intial deposition rates at different divalent salt concentrations. A detailed explanation of the QCM-D technique can found in our previous studies (Nguyen et al. 2007, Yuan et al. 2008).

Quartz sensors were supplied by Q-Sense QSX 303 silica (batches 10164, 090128-2). Before each experiment, we presoak the crystal sensors in 2% Hellmanex II (Hellma GmbH & Co. KG, Müllheim, Germany) cleaning solution for a period of time ranging from 30 to 60 min and disposed of the sensor after five uses to ensure the quality of the silica surface. The sensor was then rinsed with DI water, dried with ultrahigh-purity N_2, and oxidized in an ozone/UV chamber (Bioforce Nanosciences, Inc., Ames, IA) for 30 min. The quality of the cleaning step was then verified by measuring the QCM-D frequency and dissipation values in air and DI water.

The flow rate for experiments was 0.1 mL/min using a syringe pump (KD Scientific INC., Holliston, MA) operating in withdrawal mode. This flow rate maintains laminar flow and corresponds to a Re number of 1.0 and a Peclet number of 1.7×10^{-8}. The flow chamber of the QCM-D is a radial stagnation point flow. Before each experiment, the quartz crystal in the chamber was equilibrated with DI water at 0.1 mL/min until a stable baseline was maintained at approximated 1-2 Hz change in frequency/h for at least 20 minutes. Once the frequency signal was stabilized, 2 mL of our choice electrolyte solution ($CaCl_2$, NaCl) at the concentration of interest was injected into the sensor chamber for equilibration. Following this step, 2 mL of MS2 or RNA-free MS2 to a final optical density at 0.263 and 0.252 respectively at a wavelength 260 nm was suspended in the chosen electrolyte solution and concentration and injected into the

chamber to observe the deposition rate onto bare silica surface. For all experiments, the initial shift of frequency as a function of time, or slope of the curve at the third overtone, $f_{(3)}$, was calculated as the particle adsorption rate.

For experiments with MS2 or RNA-free MS2 attached to Poly-L-Lysine (PLL), additional steps to the procedure were as follows. After the quartz crystal in the chamber was equilibrated with DI water and achieved a stable baseline for 20 minutes, we equilibrated the crystal with 2 mL of HEPES buffer made from 10 mM N-(2-hydroxyethyl) piperazine-N'-2-ethanesulfonic acid and 100 mM NaCl (pH 6.0). The silica surface was then coated with a deposition of a layer of PLL polycations by using a solution of 200 uL PLL in 1.8 mL HEPES buffer. The silica crystal is then rinsed with 2 mL of HEPES buffer. The procedure then continues with the addition of the desired salt condition ($CaCl_2$, NaCl).

To confirm that the frequency shift represents the deposition rate, we conducted a control experiment for RNA-free MS2 deposition onto the bare silica surface in a solution of 1 mM Ca^{2+}. For these experiments we doubled the RNA-free MS2 concentration in the 2 mL and found that the initial slopes also doubled, apparent deposition of 2.99 to 5.99.

2.8 DLVO Energy Profiles

The total interaction energy between MS2 and silica plate surface was calculated using the DLVO theory, summing the repulsive electrostatic and retarded van der Waals interactions. The following expression was used to calculate the electrostatic double-layer interaction energy (Hogg et al. 1966):

$$V_{EDL}(J) = (\pi\alpha\varepsilon_0\varepsilon_r)\left\{2\psi_1\psi_2 \ln\left[\frac{1+e^{-kh}}{1-e^{-kh}}\right] + (\psi_1^2+\psi_2^2)\ln(1-e^{-2kh})\right\}$$

where ε_0 is the dielectric permittivity of free space, ε_r is the relative dielectric permittivity of water, α is the MS2 radius, k is the inverse Debye length, h is the separation distance between the MS2 virus and the silica surface, and ψ_1 and ψ_2 are the surface potentials of the MS2 virus and silica surface, respectively.

The retarded van der Waals interaction energy was calculated using the following expression (Gregory 1981):

$$V_{VDW}(J) = -\frac{Aa}{6h(1+14h/\lambda)}$$

where h is the separation distance, a is the particle radius, λ is the dielectric wavelength for water. A Hamaker constant (A) of 4x10^{-21} J was used (Penrod et al. 1996).

2.9 Error Analysis

As MS2 and RNA-free MS2 deposition onto silica was normalized by its deposition onto PLL, uncertainties needed to be combined to determine the overall uncertainty of the normalized attachment efficiency. To normalize particle deposition to silica to the deposition onto PLL, the following expression is used:

$$R = \frac{x_1}{x_2}$$

where R is the result of a specific cation concentration, x_1 is the deposition rate of particles to silica, and x_2 is the deposition rate of particles to PLL coated silica.

In order to combine uncertainties in a calculation, the following equation was used (Taylor 1997):

$$w_R = \left[\left(\frac{\partial R}{\partial x_1}w_1\right)^2 + \left(\frac{\partial R}{\partial x_2}w_2\right)^2 + \cdots + \left(\frac{\partial R}{\partial x_n}w_n\right)^2\right]^{\frac{1}{2}} = \left\{\sum_1^n \left[\left(\frac{\partial R}{\partial x_i}\right)w_i\right]^2\right\}^{\frac{1}{2}}$$

$$w_R = \left[\left(\frac{1}{x_2}w_1\right)^2 + \left(\frac{-x_1}{x_2^2}w_2\right)^2\right]^{\frac{1}{2}}$$

where w_R is the uncertainty associated with a result (R), x_1 and x_2 are independent variables with uncertainties w_1 and w_2, which in this case x_1, w_1 are the variable and uncertainty of particles attaching to silica, and x_2, w_2 are the variable and uncertainty of particles attaching to PLL. The $\left(\frac{\partial R}{\partial x_i}\right)$ is the sensitivity, or the partial derivative of R with respect to x_i.

CHAPTER 3

RESULTS AND DISCUSSION

3.1 TEM

To visually ensure that the ssRNA was removed from the MS2 bacteriophage and the capsid remained intact, we measured both the hydrodynamic diameter of the RNA-free MS2 and examined the particles using the Transmission Electron Microscope (TEM). Dynamic Light Scattering (DLS) was used to determine hydrodynamic diameter of the RNA-free MS2, which was found to be in a range of 32-36 nm. This was comparable to the stock of untreated MS2 which was found to be in a range of approximately 32-36 nm. This also is comparable to past data collected where the MS2 diameter is found to be in the 31-36 nm range (Pham et al. 2009, Gutierrez et al. 2009).

In Figure 1, where a TEM image of untreated MS2 (Figure 1A) is compared to the RNA-free MS2 (Figure 1B), we see that the untreated MS2 has a white interior due to the inability of the tungsten acetate stain to penetrate the capsid due to the ssRNA occupying the capsid. However, in the image of the RNA-free MS2 we see a dark interior due to the stain penetrating the inside of the empty capsid.

The average diameter of each particle was found to be different, the untreated MS2 had a diameter of ~27 nm where as the RNA-free MS2 had a slightly smaller diameter of ~24 nm. Potential reasoning for smaller RNA-free MS2 is that the capsid physically thinner with a smaller electrophoretic softness (see below), or steric interactions due to lack of ssRNA genome on interior to press on the compressed capsid when the capsid is no longer suspended in solution.

3.2 Electrokinetic Measurements

Electrophoretic mobility (EPM) of MS2 and RNA-free MS2 as a function of divalent cation concentrations are shown in Figure 2. The experimental data for both MS2 and RNA-free MS2 consistently show that the electrophoretic mobility of the particle becomes less negative with increasing divalent cation concentrations, as seen before in Pham et al. (2009). This indicates the association of metal ions with the MS2, with an increased screening of the electric field with an increased concentration of dissolved cations before reaching a limit in screening, as seen in Mylon et al. (2009). However, both the untreated MS2 and untreated MS2 have approximately same electrophoretic mobilities for each corresponding divalent cation concentration. For example, in a Ca^{2+} concentration of 50 mM, the electrophoretic mobility for MS2 is -0.2378 μm s^{-1} /V cm^{-1} and electrophoretic mobility for RNA-free MS2 is -0.2765 μm s^{-1} /V cm^{-1}. In Mg^{2+} concentration of 50 mM the electrophoretic mobility of MS2 is -0.30255 μm s^{-1} /V cm^{-1} and the mobility for RNA-free MS2 is -0.2655 μm s^{-1} /V cm^{-1}. Because the electrophoretic mobility of RNA-free MS2 is approximately the same as the MS2, it would suggest that the capsid controls electrophoretic mobility of the MS2 particles suspend in salt solution. There is no general trend where the MS2 or RNA-free MS2 is more negative or positive than the other.

Another interesting point of note is that while the MS2 and RNA-free MS2 are both in divalent cation solutions, the extent of which the particles approach zero in Ca^{2+} is greater than Mg^{2+}, suggesting that there are two distinct complexations occurring between the divalent cations and the capsid. This could be explained by the size of Ca^{2+} cation compared to the Mg^{2+} cation, as Ca^{2+} has a larger ionic radius than Mg^{2+} $\left(R_{Ca^{2+}} = 1.61 \text{ Å},\ R_{Mg^{2+}} = 0.92 \text{ Å}\right)$, it can be expected to have a stronger interaction with the MS2 capsid (Ahn et al. 2008, Newman et al.

1994, Wu et al. 1996). Mg^{2+} being the smaller cation, it has a stronger hydration sphere around it and therefore can only make weaker complexes, where as the larger Ca^{2+} has a looser hydration sphere and can more easily exchange the water to create stronger complexes.

The electrophoretic mobility of MS2 and RNA-free MS2 as a function of monovalent cation (Na^{+}) concentrations is shown in Figure 3. The experimental data for both MS2 and RNA-free MS2 once again shows that the electrophoretic mobility of a particle becomes less negative with an increasing concentration. However, in the case of monovalent cations, the increase is lower than Ca^{2+} and Mg^{2+}, even at the same ionic strength. This may be explained by monovalent cations such as Na^{+} just provides charge screening, where as the divalent cations forms complexations with the MS2 capsid.

Measuring the electrophoretic mobility of MS2 and RNA-free MS2 as a function of monovalent cation concentrations were used to determine the particle's electrophoretic softness using Ohshima's model (Ohshima 1995) for soft particles. The electrophoretic softness, $1/\lambda$, the width of the soft layer around a particle, was found to be 2.1 nm for MS2 and 1.6 nm for RNA-free MS2. This suggests that the "soft" region of the RNA-free MS2 capsid is smaller than the MS2 and may behave as a harder particle.

The isoelectric point (IEP) of MS2 and RNA-free MS2 sample stored in 1 mM NaCl was found by measuring electrophoretic mobility at a range of pH from 2.7 to 9.6. The IEP is determined as the pH condition at which electrophoretic mobility changes from positive to negative. As shown in Figure 4, the IEP for MS2 stock is approximately 3.4 in 1 mM NaCl solution, and the IEP for RNA-free MS2 stock is approximately 3.2 in 1 mM NaCl solution. IEP for MS2 has been reported as 3.5 by Penrod et al. (1996), 2.9 by Overby et al. (1966), and 3.8 by Schaldach et al. (2006), and 3.4 by Langlet et al (2008) in a $NaNO_3$ buffer. We find that

our MS2 stock is in agreement with previous studies and that the result for RNA-free MS2 to be approximately similar to the untreated MS2.

3.3 Aggregation Kinetics Measurements

Time Resolved Dynamic Light Scattering was used to measure the kinetics of virus/virus aggregation in both monovalent (Na^+) and divalent (Ca^{2+}, Mg^{2+}) cation conditions. In the monovalent condition, it was found that there was no significant aggregation of MS2 or RNA-free MS2 even at 600 mM Na^+, as seen in Figure 5 by the average hydrodynamic diameter not increasing more than 30% beyond the original diameter ~36 nm, suggesting that Na^+ does not have a significant impact on the energy barrier that keep the MS2 capsids from aggregating in natural conditions.

Observing that there is no significant aggregation of MS2 or RNA-free MS2 in Na^+ solution, even in an ionic strength as high as 600 mM, it is found that this behavior does not agree with the DLVO calculations for virus-virus interaction in Na^+, provided in Table 1. The DLVO calculations in Table 1 predict that there would be significant aggregation at approximately 150-300 mM Na^+ where there is no energy barrier. As there is no significant aggregation at higher Na^+ concentrations, steric repulsion may be the dominant force in preventing MS2 and RNA-free MS2 from aggregating, which is not accounted for in DLVO.

Figure 6 presents the attachment efficiency as a function of divalent cation concentrations. In both cases of Ca^{2+} and Mg^{2+}, there is a trend of increasing attachment efficiency until ~10 mM concentration, at which point the attachment efficiency remains relatively stable with increasing concentration. This would indicate that the particles have reached the critical coagulation concentration (CCC), at which point the aggregation is rapid and becomes diffusion limited. The effect of divalent cations showing a substantial effect on the

destabilization of MS2 in suspension was seen before in Mylon et al. (2009) where it was proposed that the possible mechanisms for virus aggregation in the presence of divalent cations involves both charge neutralization and cation bridging due to complexation of the divalent cation to the negatively charged functional groups on the MS2 surface or complexation of divalent cations induce changes in the MS2 capsid, affecting the structural characteristics.

It can be seen in both figures that both the untreated MS2 and RNA-free MS2 both have similar attachment efficiencies for a given salt condition, be it monovalent or divalent. For example, at 10 mM Ca^{2+}, the attachment efficiency of MS2 is 0.47505 and for RNA-free MS2 it is 0.65048. With the given sensitivity of equipment, this suggests that the ssRNA inside the capsid has no notable influence on the aggregation of capsids, and that the metal ions primarily complex with the capsid and destabilize the energy barrier to allow for virus/virus aggregation to occur.

Comparing the virus-virus DLVO calculations for Ca^{2+} in Table 2 and Mg^{2+} in Table 3 to the trend observed in Figure 6, we see that the DLVO makes a fair approximation of the behavior. At the point where no energy barrier is calculated, 10 mM is the approximate location of the CCC. This is in agreement as there is no longer any energy barrier to repel the virus particles from each other, rapid aggregation may occur. It can also be observed for the case of 5 mM Ca^{2+} the DLVO has a relatively low energy barrier and the attachment efficiency is about the same as the plateau. However, DLVO is not an optimal model for predicting the behavior of the capsids as it does not take into account the complexation of cations to the capsid surface, or the steric forces of the capsid.

3.4 QCM-D Measurements

Untreated MS2 and RNA-free MS2 deposition onto PLL-coated silica surface as a function of cation concentration are shown in Figure 7A for Na^+ and Figure 8A for Ca^{2+}. We define that MS2/PLL deposition is favorable as the MS2 capsid is negatively charged and the PLL is positively charged, creating an attractive layer for which the particles can deposit upon. The apparent deposition rate for both MS2 and RNA-free MS2 are shown to be relatively stable for the range of Na^+ concentrations (10-300 mM), while the apparent deposition rate for MS2 and RNA-free MS2 showed a decrease in deposition rates with an increase of Ca^{2+} concentration (0.3 mM to 200 mM). The behavior of stability while depositing MS2 to PLL has been demonstrated before Pham (2009), and Elimelech (1991, 1994) states that deposition rates of negatively charged colloidal particles onto a positively charged collector should be stable or slightly decreased with increasing electrolyte concentrations when no energy barrier exists between the particles and the collector. This second behavior is demonstrated by MS2 and RNA-free MS2 in high Ca^{2+} concentrations.

The cause of the higher deposition at lower cation concentrations than that of higher cation concentrations is that the electrical double layer produced by the MS2 capsid is thicker in a low ionic strength, or low cation concentration, and decreases with an increasing ionic strength. The electrical double layer is the influential layer in deposition onto an attractive surface such as PLL, and as the ionic strength increases, the electrical double layer thickness decreases, thus decreasing the radius of influence and decreasing the rate at which MS2 capsids deposit onto the surface (Elimelech 1991).

The apparent deposition rates of MS2 and RNA-free MS2 to silica as a function of cation concentration can be seen in Figure 7B for Na^+ and Figure 8B for Ca^{2+}. It can be seen that with

increasing cation concentration, that the apparent deposition of untreated MS2 and RNA-free MS2 increases. This can be attributed to the effect of cations destabilizing the MS2 capsid in suspension as mentioned before for aggregation, caused by charge screening of the capsid, or complexation of the capsid with the Ca^{2+} (Mylon et al. 2009).

The attachment efficiency (α) of MS2 and RNA-free MS2 to silica as a function of cation concentration can be seen in Figure 7C for Na^{+} and Figure 8C for Ca^{2+}. To normalize MS2/Silica results to obtain attachment efficiency, we define that MS2/PLL deposition is favorable as both MS2 and silica are negatively charged, while PLL is positively charged. As seen in the apparent deposition of MS2 and RNA-free MS2, the attachment efficiency of both particles increases as the cation concentration increases. In Figure 7C, the highest attachment efficiency obtained is 0.1332 for MS2 at 300 mM Na^{+} and 0.3147 for RNA-free MS2 at 300 mM Na^{+}. Neither particles in Na^{+} solution reaches an attachment efficiency of 1.0, indicating the possibility of steric hinderances preventing attachment even at increasing ionic strengths. In Figure 8C, the highest attachment efficiency obtained is 0.3132 for MS2 at 200 mM Ca^{2+} and 1.2232 for RNA-free MS2 at 200 mM Ca^{2+}. In this case, MS2 never reaches an attachment efficiency of 1.0, and RNA-free MS2 does reach 1.0 and surpass at the higher Ca^{2+} concentration, again indicating that there may be steric forces at work.

In both cases, it can be seen that both untreated MS2 and RNA-free MS2 behave in a very similarly with approximately the same increase in attachment efficiency with the increase of cation concentration. However, it should be noted that the RNA-free MS2 deposits at a slightly higher efficiency that MS2 each time. As calculated in Figure 3 using the Ohshima model, the electrophoretic softness of RNA-free MS2 is less than that of the MS2, indicating that the RNA-free MS2 particle should behave as a slightly harder particle. This evidence is supported by the

increased attachment efficiency of RNA-free MS2 over MS2, as there steric repulsion should be less for the RNA-free MS2 than the MS2

Table 4 presents the DLVO calculated energy barriers between MS2 or RNA-free MS2 and the silica surface for deposition. The DLVO predicts that for both Na^+ and Ca^{2+} concentrations at 100 mM, there should be no energy barrier, however it can be seen in Figure 7C and 8C, that the attachment efficiency of MS2 and RNA-free MS2 is not α=1.0 and in the case of Na^+ in Figure 8C, the attachment efficiency never reaches α=1.0. The reasoning for the MS2 and RNA-free MS2 not reaching a higher attachment efficiency than what may predicted from DLVO is that DLVO only takes into account the van der Waals forces and electrostatic forces, and not the steric forces involved, which may be the largest influence on the attachment efficiency of both particles.

CHAPTER 4

CONCLUSION

The interfacial behavior of the bacteriophage MS2 capsid was investigated in order to determine the influence of the ssRNA core on surface behavior. MS2 being a well studied model waterborne virus and nanoparticle, it is a valuable tool to help understand how the electrostatics of the core can affect the overall surface characteristics of a particle. Removing the genome from the MS2 and forming an empty capsid, a virus like particle, provides us the opportunity to physically observe and measure the interactions of the MS2 capsid simultaneously with MS2 for direct comparison.

After determining that the empty MS2 capsid was intact, we observed that the RNA-free MS2 showed no significant difference compared to untreated MS2 while measuring the electrophoretic mobility and virus/virus aggregation of the particles in suspensions containing varying concentrations of Na^{+}, Ca^{2+}, and Mg^{2+}. Using the Ohshima model to determine the electrophoretic softness of the soft particles, it was found that RNA-free MS2 is a slightly harder particle than untreated MS2. The deposition kinetics of RNA-free MS2 and untreated MS2 to a silica surface showed similar trends in Na^{+} and Ca^{2+}, it was found that the RNA-free MS2 attachment efficiency was greater than untreated MS2 to be significant. This is attributed to the RNA-free MS2 being the harder particle and therefore a better deposition efficiency, so the difference between the two particles in deposition is due to steric effects more so than electrostatic.

In the case of aggregation and deposition, it is found that the DLVO calculations were not an accurate predictor of the outcome of what ionic strength significant aggregation would occur, or when the attachment efficiency of deposition would reach its critical coagulation

concentration. This is due to the fact that the DLVO theory only approximates the electrostatic and van der Waals forces as simple separate forces, and the calculations are not meant for "soft" particle where there exists steric and electrosteric interactions, or the effects of complexation of cations with the interphase of the capsid.

In conclusion, our work suggests that the protein capsid of MS2 virus is a more dominant force than the single strand RNA inside with respect to the electrostatic forces. However, the QCM used in our work is much more sensitive than the DLS used. Future work could potentially be to measure the electrostatics of these two particles with a more accurate instrument.

FIGURES AND TABLES

Figure 1

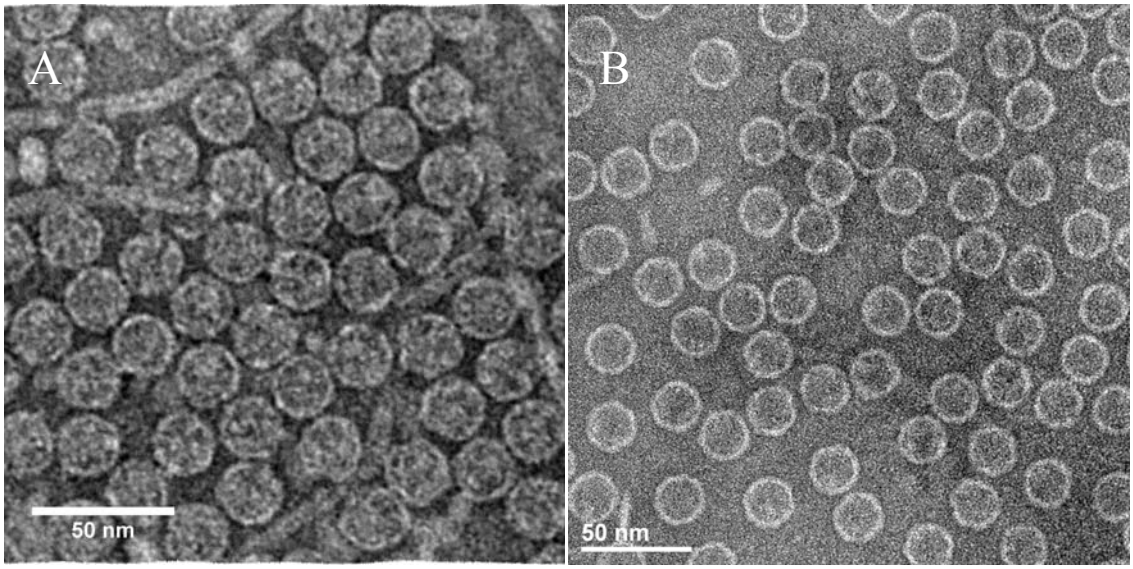

Figure 1: Cryo-TEM image of untreated MS2 bacteriophage (a) and cryo-TEM image of RNA-free MS2 bacteriophage (b). Tungsten acetate was used as a stain for both particles. The treated RNA-free MS2 particles contain dark interiors due to the penetration of stain inside the empty capsid, where as the wild type MS2 appears white due to the stain being unable to penetrate the capsid because of the presence of RNA.

Figure 2

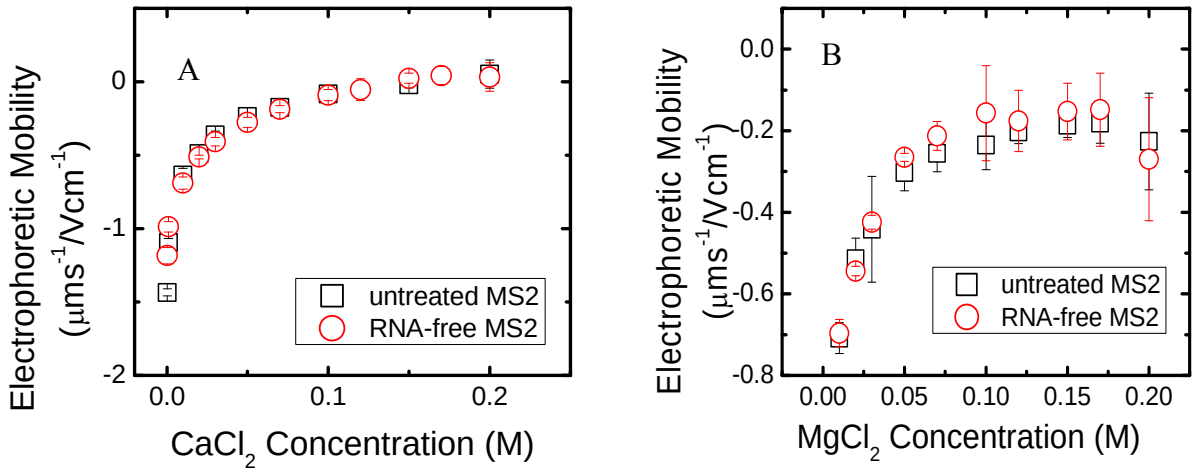

Figure 2: Electrophoretic mobility of MS2 and RNA-free MS2 in Ca^{2+} (a) and Mg^{2+} (b) shown as a function of divalent cation concentration. Both MS2 and RNA-free MS2 start with negative electrophoretic mobility and approach zero with increasing ionic strength. However, when suspended in Ca^{2+}, the MS2 and RNA-free MS2 have a closer approach to zero than the MS2 and RNA-free MS2 suspended in Mg^{2+}.

Figure 3

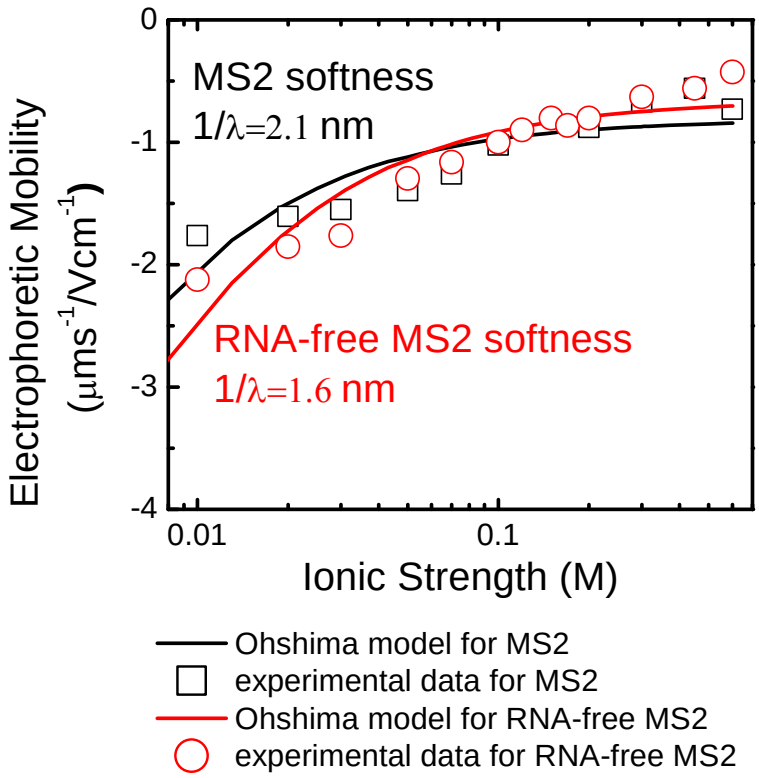

Figure 3: Electrophoretic mobility of MS2 and RNA-free MS2 as a function of ionic strength, using NaCl, at constant pH. This was used to calculate the electrophoretic softness of the MS2 and RNA-free MS2, which were found to be 2.1 nm and 1.6 nm respectively using the Ohshima model (Ohshima 1995). This indicates that the RNA-free MS2 particles were found to be slightly harder particles than the untreated MS2.

Figure 4

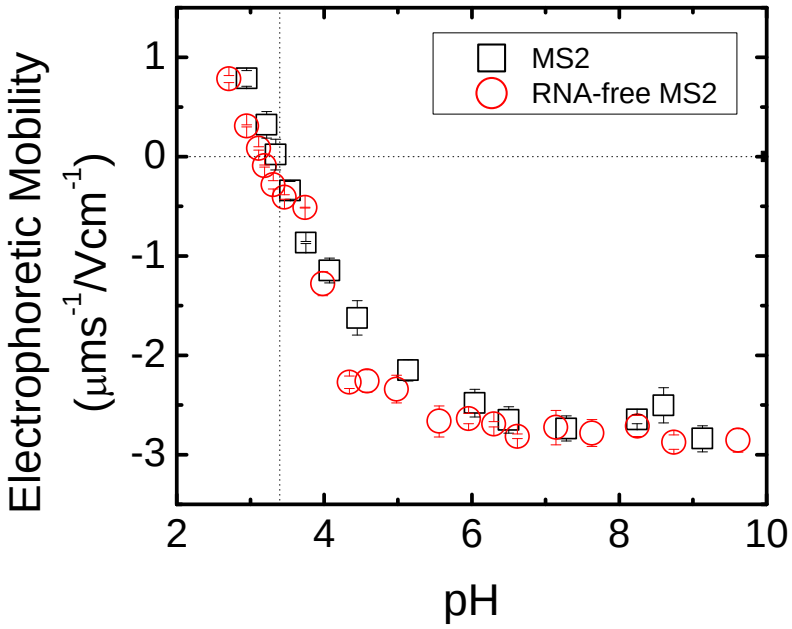

Figure 4: Electrophoretic mobility of wild-type MS2 and hollow MS2 at a constant 1 mM NaCl solution while varying the pH with HCl and NaOH. The isoelectric point was found not to vary significantly between the two types of MS2, as the wild-type MS2 and hollow MS2 was found to be 3.4 and 3.2 respectively.

Figure 5

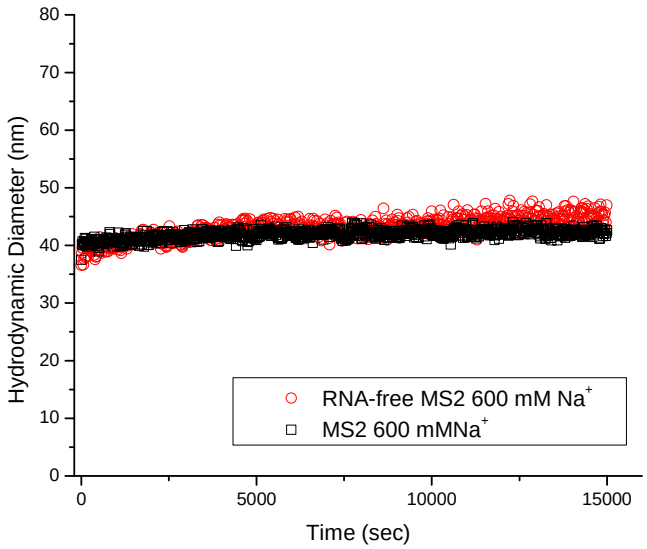

Figure 5: Time resolved dynamic light scattering of MS2 and RNA-free MS2 experiencing aggregation at 600 mM NaCl. Although the aggregation kinetic rates are similar in magnitude, the Kapp of RNA-free MS2 was slightly higher, Kapp of 0.0003 compared to untreated MS2 Kapp 0.0001, suggesting that MS2 behaves as a softer particle.

Figure 6

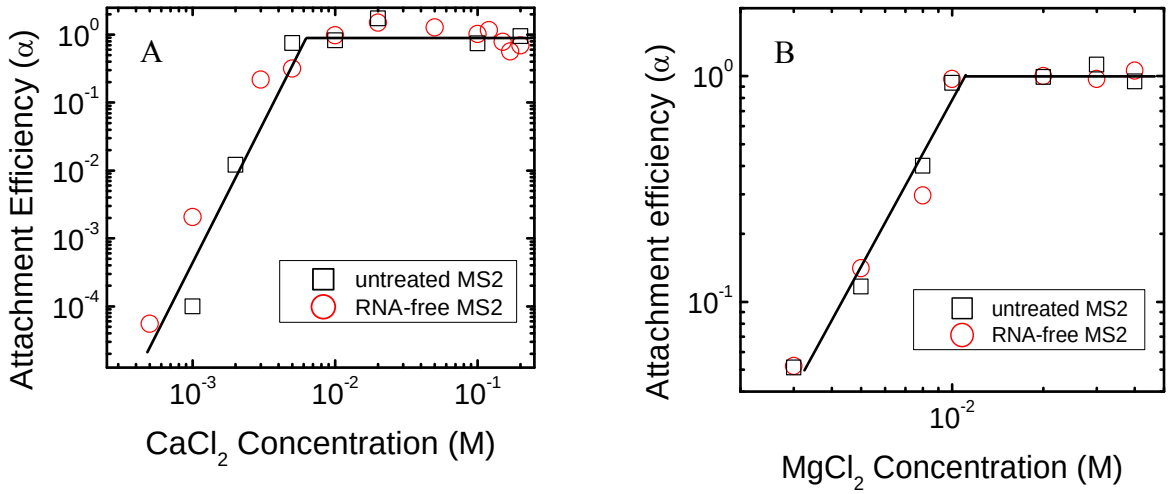

Figure 6: Aggregation bacteriophage particles of MS2 and hollow MS2 were similar in the presence of Ca^{2+} (a) and Mg^{2+} (b), measured by time resolved dynamic light scattering. The critical coagulation concentration (CCC) occurs approximately 10 mM for both types of particles in the presence of Ca^{2+} and Mg^{2+}, after which rapid aggregation occurs.

Figure 7

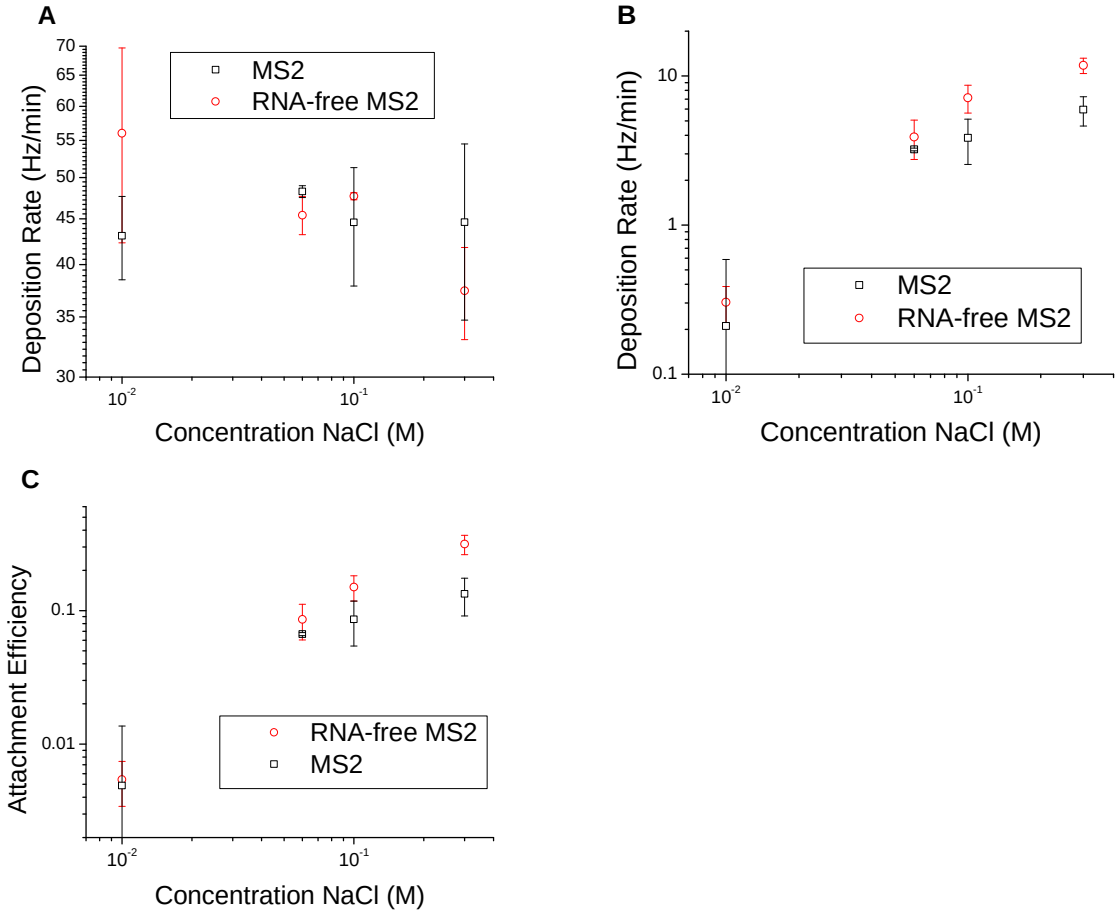

Figure 7: Experimentally measured apparent deposition rates for MS2 and RNA-free MS2 onto PLL in the presence of Na^+ (a), apparent deposition rates for MS2 and RNA-free MS2 onto silica (b), and normalized attachment efficiency for MS2 and RNA-free MS2 (c), all using the Quartz-Crystal Microbalance with Dissipation. It can be seen that in the case of favorable deposition of MS2 capsid to PLL, the apparent rate of deposition stays approximately the same with increasing Na^+ concentration. However, in the case of unfavorable deposition of MS2 capsid to silica, the apparent rate of deposition increases with increasing Na^+. For the normalized attachment efficiency, the efficiency increases as the Na^+ concentration increases, with the RNA-free MS2 showing a higher affinity than MS2. This could be attributed to the smaller electrophoretic softness of RNA-free MS2 making it behave as a harder particle.

Figure 8:

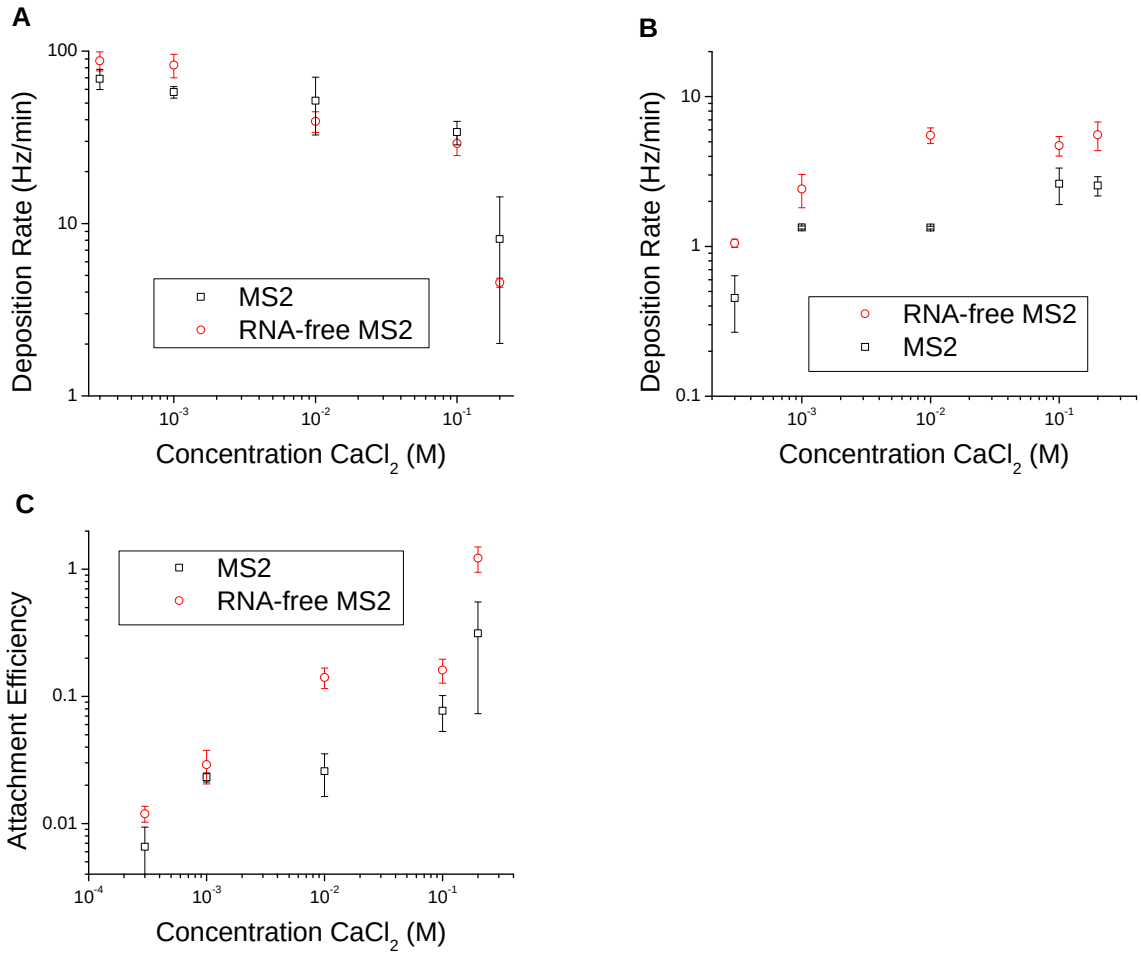

Figure 8: Experimentally measured apparent deposition rates for MS2 and RNA-free MS2 onto PLL in the presence of Ca^{2+} (a), apparent deposition rates for MS2 and RNA-free MS2 onto silica (b), and normalized attachment efficiency for MS2 and RNA-free MS2 (c), all using the Quartz-Crystal Microbalance with Dissipation. It can be seen that in the case of favorable deposition of MS2 capsid to PLL, the apparent rate of deposition decreases with increasing Ca^{2+} concentration. However, in the case of unfavorable deposition of MS2 capsid to silica, the apparent rate of deposition increases with increasing Ca^{2+}. For the normalized attachment efficiency, the efficiency increases as the Ca^{2+} concentration increases, with the RNA-free MS2 showing a higher affinity than MS2. This could be attributed to the smaller electrophoretic softness of RNA-free MS2 making it behave as a harder particle.

Table 1: Energy barrier values for MS2 and RNA-free MS2 aggregating in a homogenous solution in the presence of Na^+, calculated by DLVO. The haymaker constant (A) of $4x10^{-21}$ J was used (Penrod et al. 1996). Diameters used for each particle were 36.4 nm for MS2, 36.6 nm for RNA-free MS2. Whenever "no barrier" is present, it indicates that no energy barrier was present in the DLVO calculation. As it can be seen in the Na^+ calculations, there were no energy barrier values at the 150-300 mM range.

Na+ Conc. (mM)	Energy barrier (kT)	
	MS2	RNA-free MS2
10	6.55	11.78
20	4.10	6.16
30	3.10	4.57
50	1.67	1.21
70	0.77	0.45
100	-0.14	-1.16
150	-0.22	No Barrier
300	No Barrier	No Barrier
600	No Barrier	No Barrier

Table 2: Energy barrier values for MS2 and RNA-free MS2 aggregating in a homogenous solution in the presence of Ca^{2+}, calculated by DLVO. The haymaker constant (A) of $4x10^{-21}$ J was used (Penrod et al. 1996). Diameters used for each particle were 36.4 nm for MS2, 36.6 nm for RNA-free MS2. Whenever "no barrier" is present, it indicates that no energy barrier was present in the DLVO calculation. As it can be seen in the Ca^{2+} calculations, there was no energy barrier present at 10 mM.

Ca2+ Conc. (mM)	Energy barrier (kT)		Attachment Efficiency (α)	
	MS2	RNA-free MS2	MS2	RNA-free MS2
1	1.72	1.29	9.92E-05	0.00206
2	1.26		0.0121	
3		0.71		0.2178
5	0.44	0.36	0.7527	0.31748
10	No Barrier	No Barrier	0.82103	0.98287
20	No Barrier	No Barrier	1.72828	1.51098
50	No Barrier	No Barrier		1.27522
100	No Barrier	No Barrier	0.74844	1.01864
150	No Barrier	No Barrier		0.78438
200	No Barrier	No Barrier	0.94955	0.6955

Table 3: Energy barrier values for MS2 and RNA-free MS2 aggregating in a homogenous solution in the presence of Mg^{2+}, calculated by DLVO. The haymaker constant (A) of $4x10^{-21}$ J was used (Penrod et al.1996). Diameters used for each particle were 36.4 nm for MS2, 36.6 nm for RNA-free MS2. Whenever "no barrier" is present, it indicates that no energy barrier was present in the DLVO calculation. As it can be seen in the Mg^{2+} calculations, there was no energy barrier present at 10 mM.

Mg2+ Conc. (mM)	Energy barrier (kT)		Attachment Efficiency (α)	
	MS2	RNA-free MS2	MS2	RNA-free MS2
3			0.05106	0.05185
5			0.11672	0.14074
8			0.40122	0.2963
10	No Barrier	No Barrier	0.93374	0.97037
20	No Barrier	No Barrier	0.9921	1
30	No Barrier	No Barrier	1.12584	0.97037
40	No Barrier	No Barrier	0.94833	1.05926

Table 4: Values of energy barriers for MS2 and RNA-free MS2 deposited onto the Silica surface in the presence of Na^{+} and Ca^{2+}. The haymaker constant (A) of $4x10^{-21}$ J was used (Penrod et al. 1996). Diameters used for each particle were 36.4 nm for MS2, 36.6 nm for RNA-free MS2. Whenever "no barrier" is present in the table, it indicates that no energy barrier was present in the DLVO calculation.

Na+ Conc. (mM)	Energy barrier (kT)		Ca2+ Conc. (mM)	Energy barrier (kT)	
	MS2	RNA-free MS2		MS2	RNA-free MS2
10	13.597	17.909	0.3	11.285	8.14
60	0.372	0.237	1	6.149	5.098
100	No Barrier	No Barrier	10	-0.014	0.192
300	No Barrier	No Barrier	100	No Barrier	No Barrier
			200	No Barrier	No Barrier

REFERENCES

Abbaszadegan, M., M. Lechevallier, and C. Gerba. 2003. Occurrence of viruses in US groundwaters. Journal / American Water Works Association 95, (9): 107-120.

Adams, M., 1959. Bacteriophages. IntersciencePublishers,NewYork.

Ahn, W. -Y, A. G. Kalinichev, and M. M. Clark. 2008. Effects of background cations on the fouling of polyethersulfone membranes by natural organic matter: Experimental and molecular modeling study. Journal of Membrane Science 309, (1-2): 128-140.

Brown, S.D., J.D. Fiedler, and M.G. Finn, 2009. Assembly of Hybrid Bacteriophage Q beta Virus-like Particles. Biochemistry. 48(47): p. 11155-11157.

Chen, K.L., S.E. Mylon, and M. Elimelech, 2006. Aggregation kinetics of alginate-coated hematite nanoparticles in monovalent and divalent electrolytes. Environmental Science & Technology. 40(5): p. 1516-1523.

Chen, K. L., and M. Elimelech. 2006. Aggregation and deposition kinetics of fullerene (C60) nanoparticles. Langmuir 22, (26): 10994-11001.

Dowd, S. E., S. D. Pillai, S. Wang, and M. Y. Corapcioglu. 1998. Delineating the specific influence of virus isoelectric point and size on virus adsorption and transport through sandy soils. Applied and Environmental Microbiology 64, (2): 405-410.

Elimelech, M. 1991. Kinetics of capture of colloidal particles in packed beds under attractive double layer interactions. Journal of colloid and interface science 146, (2): 337-352.

Elimelech, M. 1994. Effect of particle size on the kinetics of particle deposition under attractive double layer interactions. Journal of colloid and interface science 164, (1): 190-199.

Elimelech, M., J. Gregory, X. Jia, and R. A. Williams, Particle Deposition and Aggregation: Measurement, Modelling and Simulation, Butterworth-Heinemann, Oxford, 1995.

Fischlechner, M., and E. Donath. 2007. Viruses as building blocks for materials and devices. Angewandte Chemie - International Edition 46, (18): 3184-3193.

Floyd, R. and D.G. Sharp, 1979. Viral Aggregation - Buffer Effects In The Aggregation Of Poliovirus And Reovirus At Low And High pH. Applied and Environmental Microbiology. 38(3): p. 395-401.

Floyd, R. and D.G. Sharp, 1978. Viral Aggregation - Effects Of Salts On Aggregation Of Poliovirus And Reovirus At Low-pH. Applied and Environmental Microbiology. 35(6): p. 1084-1094.

Floyd, R. and D.G. Sharp, 1977. Aggregation Of Poliovirus And Reovirus By Dilution In Water. Applied and Environmental Microbiology. 33(1): p. 159-167.

Garcea, R.L. and L. Gissmann, 2004. Virus-like particles as vaccines and vessels for the delivery of small molecules. Current Opinion in Biotechnology. 15(6): p. 513-517.

Gregory, J., 1981. Approximate Expressions for Retarded Van der Waals Interaction. J. Colloid Interface Sci., 83 (1), 138–145.

Gutierrez, L., X. Li, J. Wang, G. Nangmenyi, J. Economy, T. B. Kuhlenschmidt, M. S. Kuhlenschmidt, and T. H. Nguyen. 2009. Adsorption of rotavirus and bacteriophage MS2 using glass fiber coated with hematite nanoparticles. Water research 43, (20): 5198-5208.

Gutierrez, L., S. E. Mylon, B. Nash, and T. H. Nguyen. 2010. Deposition and aggregation kinetics of rotavirus in divalent cation solutions. Environmental Science and Technology 44, (12): 4552-4557.

Herath, G., K. Yamamoto, and T. Urase, 1999. Removal of viruses by microfiltration membranes at different solution environments. Water Science and Technology. 40(4-5): p. 331-338.

Hogg, R., T. W. Healy, and D. W. Fuerstenau. 1966. Mutual coagulation of colloidal dispersions. Transactions of the Faraday Society 62: 1638-1651.

Hooker, J. M., E. W. Kovacs, and M. B. Francis. 2004. Interior surface modification of bacteriophage MS2. Journal of the American Chemical Society 126, (12): 3718-3719.

Ishikawa, Y., Y. Katoh, and H. Ohshima. 2005. Colloidal stability of aqueous polymeric dispersions: Effect of pH and salt concentration. Colloids and Surfaces B: Biointerfaces 42, (1): 53-58.

Kitis, M., Lozier, J.C., Kim, J.H., Mi, B.X., Marinas, B.J., 2003. Microbial removal and integrity monitoring of RO and NF membranes. Journal of the American Water Works Association 95 (12), 105–119.

Kuzmanovic, D. A.; Elashvili, I.; Wick, C.; O'Connell, C.; Krueger, S., 2003. Bacteriophage MS2: Molecular weight and spatial distribution of the protein and RNA components by small-angle neutron scattering and virus counting. Structure, 11 (11), 1339-1348.

Labelle, R.L. and C.P. Gerba, 1979. Influence Of Ph, Salinity, And Organic-Matter On The Adsorption Of Enteric Viruses To Estuarine Sediment. Applied and Environmental Microbiology. 38(1): p. 93-101.

Lance, J.C. and C.P. Gerba, 1984. Effect Of Ionic Composition Of Suspending Solution On Virus Adsorption By A Soil Column. Applied and Environmental Microbiology. 47(3): p. 484-488.

Langlet, J., F. Gaboriaud, J. Duval, and C. Gantzer. 2008. Aggregation and surface properties of F-specific RNA phages: Implication for membrane filtration processes. Water research 42, (10-11): 2769-2777.

Langlet, J., F. Gaboriaud, C. Gantzer, and J. F. L. Duval. 2008. Impact of chemical and structural anisotropy on the electrophoretic mobility of spherical soft multilayer particles: The case of bacteriophage MS2. Biophysical journal 94, (8): 3293-3312.

Laufer, B., N.F. Steinmetz, V. Hong, M. Manchester, H. Kessler, M.G. Finn, 2009. Guiding Vlp's The Right Way: Coating Of Virus Like Particles With Peptidic Integrin Ligands. Biopolymers. 92(4): p. 323-323.

Legendre, D.; Fastrez, J., 2005. Production in Saccharomyces cerevisiae of MS2 virus-like particles packaging functional heterologous mRNAs. Journal of Biotechnology**,** 117 (2), 183-194.

Lee, Y. J., H. Yi, W. -J Kim, K. Kang, D. S. Yun, M. S. Strano, G. Ceder, and A. M. Belcher. 2009. Fabricating genetically engineered high-power lithium-ion batteries using multiple virus genes. Science 324(5930): p. 1051-1055.

Lipson, S.M. and G. Stotzky, 1984. Effect Of Proteins On Reovirus Adsorption To Clay-Minerals. Applied and Environmental Microbiology, 48(3): p. 525-530.

Mylon, S. E., C. I. Rinciog, N. Schmidt, L. Gutierrez, G. C. L. Wong, and T. H. Nguyen. 2010. Influence of salts and natural organic matter on the stability of bacteriophage MS2. Langmuir 26, (2): 1035-1042.

Nel, A. E., L. Mädler, D. Velegol, T. Xia, E. M. V. Hoek, P. Somasundaran, F. Klaessig, V. Castranova, and M. Thompson. 2009. Understanding biophysicochemical interactions at the nano-bio interface. Nature Materials 8, (7): 543-557.

Newman, J. K., and C. L. McCormick. 1994. Water-soluble copolymers. 52. sodium-23 NMR studies of ion-binding to anionic polyelectrolytes: Poly(sodium 2-acrylamido-2-methylpropanesulfonate), poly(sodium 3-acrylamido-3-methylbutanoate), poly(sodium acrylate), and poly(sodium galacturonate). Macromolecules 27, (18): 5114-5122.

Nguyen, T. H.; Chen, K. L., 2007. Role of divalent cations in plasmid DNAadsorption to natural organic matter-coated silica surface. Environ. Sci. Technol., 41 (15), 5370–5375.

Nguyen, T. H.; Elimelech, M., 2007. Adsorption of plasmid DNA to a natural organic matter-coated silica surface: Kinetics, conformation, and reversibility. Langmuir, 23 (6), 3273–3279.

Nguyen, T. H.; Elimelech, M., 2007. PlasmidDNAadsorption on silica: Kinetics and conformational changes in monovalent and divalent salts. Biomacromolecules, 8 (1), 24–32.

Ohshima, H. 1995. Electrophoretic mobility of soft particles. Colloids and Surfaces A: Physicochemical and Engineering Aspects 103, (3): 249-255.

Overby, L. R., G. H. Barlow, R. H. Doi, M. Jacob, and S. Spiegelman. 1966. Comparison of two serologically distinct ribonucleic acid bacteriophages. I. properties of the viral particles. Journal of Bacteriology 91, (1): 442-448.

Penrod, S. L.; Olson, T. M.; Grant, S. B., 1996. Deposition kinetics of two viruses in packed beds of quartz granular media. Langmuir, 12 (23), 5576–5587.

Pham, M., E. A. Mintz, and T. H. Nguyen. 2009. Deposition kinetics of bacteriophage MS2 to natural organic matter: Role of divalent cations. Journal of colloid and interface science 338, (1): 1-9.

Schaldach, C. M., W. L. Bourcier, H. F. Shaw, B. E. Viani, and W. D. Wilson. 2006. The influence of ionic strength on the interaction of viruses with charged surfaces under environmental conditions. Journal of colloid and interface science 294, (1): 1-10.

Taylor, John. An Introduction to Error Analysis. Sausalito: University Science Books, 1997.

Thompson, S.S. and M.V. Yates, 1999. Bacteriophage inactivation at the air-water-solid interface in dynamic batch systems. Applied and Environmental Microbiology. 65(3): p. 1186-1190.

Udit, A. K., C. Everett, A. J. Gale, J. R. Kyle, M. Ozkan, and M. G. Finn. 2009. Heparin antagonism by polyvalent display of cationic motifs on virus-like particles. ChemBioChem 10, (3): 503-510.

Yoder, J., V. Roberts, G.F. Craun, V. Hill, L. Hicks, N.T. Alexander, V. Radke, R.L. Calderon, M.C. Hlavsa, M.J. Beach, S.L. Roy, 2008. Surveillance for Waterborne Disease and Outbreaks Associated with Drinking Water and Water not Intended for Drinking --- United States, 2005—2006, CDC.

Yuan, B., M. Pham, and T. H. Nguyen. 2008. Deposition kinetics of bacteriophage MS2 on a silica surface coated with natural organic matter in a radial stagnation point flow cell. Environ. Sci. and Technol., 42, (20): 7628-7633.

Wu, S. L., K. A. Johnson, and W. DeW Horrocks Jr. 1997. Kinetics of formation of Ca2+ complexes of acyclic and macrocyclic poly(amino carboxylate) ligands: Bimolecular rate constants for the fully-deprotonated ligands reveal the effect of macrocyclic ligand constraints on the rate-determining conversions of rapidly-formed intermediates to the final complexes. Inorganic chemistry 36, (9): 1884-1889.